Resonance Raman scattering in photonic band-gap materials

Mesfin Woldeyohannes,[1] Sajeev John,[1] and Valery I. Rupasov[1,2]
[1]*Department of Physics, University of Toronto, 60 St. George Street, Toronto, Ontario, Canada M5S 1A7*
[2]*Landau Institute for Theoretical Physics, Moscow, Russia*
(Received 4 May 2000; published 13 December 2000)

We study the resonance Raman scattering of light from a three-level atom embedded in a photonic band-gap material or in a frequency dispersive medium whose photon spectrum exhibits a gap due to photon coupling to medium excitations such as excitons and optical phonons. We demonstrate that the one-particle spectrum of the system consists of either a continuous part with energy lying outside the gap or a single discrete mode with energy lying inside the gap. The discrete mode, which occurs when both of the allowed atomic transitions of the Λ configuration lie inside the gap, can be treated as a photon-atom bound state in which the radiation is localized in the vicinity of the atom. In the case of the continuous spectrum, the Rayleigh and Stokes lines are shifted as well as narrowed (or broadened) as the corresponding transition frequencies are shifted relative to the upper band edge, providing a distinctive experimental signature of atom-photon interactions near a photonic band edge.

DOI: 10.1103/PhysRevA.63.013814 PACS number(s): 42.50.Gy, 42.70.Qs

I. INTRODUCTION

The prediction [1,2] and experimental observation [3] of photonic band-gap (PBG) materials have opened a door to new effects in the quantum optics of atom-photon interactions. These materials are artificial periodic dielectric structures exhibiting a gap in the photon density-of-states for all directions of electromagnetic propagation. This absence of propagating photon states within the photonic band gap leads to the inhibition of single-photon spontaneous emission [1], classical light localization [2,4], photon-atom bound state [5], fractionalized single atom inversion [6], and anomalous vacuum Rabi splitting [6,7]. In the presence of many atoms, it also leads to anomalously fast collective spontaneous emission rates near the band edge [8] and photon hopping conduction deeper within the gap [9]. The sharp variation of the density of photon states near the band edges leads to non-Markovian atom-photon interactions [10] and may be used to advantage for fast optical switching and optical transistor action [11,12] at low-field intensities.

The photon-atom bound state describes the one-particle spectrum of an atom plus photon system with an eigenfrequency lying within the band gap. A photon emitted by an atom in such a dressed state tunnels within the PBG material on length scale given by the localization length, only to be Bragg reflected back to the emitting atom and re-excite it. Experimental investigation of the photon-atom bound state have been hampered by the fact that its eigenfrequency lies within the PBG, forcing the mode-light coupling to be off resonance. A search for optical phenomena that exhibit spectroscopic signatures of a photon-atom bound state and provides experimental information on the electromagnetic spectrum in the vicinity of the gap is an important issue in the characterization of PBG materials.

In this paper we study the problem of Raman scattering for a three-level atom in the Λ configuration embedded in a PBG material. Using an exact solution of the one-particle Schrödinger equation, we demonstrate that the spectrum of the system consists of both a continuous part with energy lying outside the gap and a single discrete mode (provided the two allowed atomic transitions of the Λ configuration lie inside the gap) with energy lying inside the gap. The discrete mode can be treated as a photon-atom bound state in which the radiation is localized in the vicinity of the atom. In contrast to the case of a two-level atom [6,13–15], in the present case there are two scattering channels, the elastic (Rayleigh) and inelastic (Stokes or anti-Stokes) channels. The radiation field is bound to the atom as a result of two-channel scattering, while the atom switches between the ground level and the next excited level via the upper most excited level. In the case of the continuous spectrum, the Rayleigh and Stokes lines are shifted as well as narrowed (or broadened) as the corresponding transition frequencies are shifted relative to the upper photonic band edge.

It is well known that a frequency gap for propagating photons also exists in certain natural dielectric materials. Unlike artificial PBG materials, the gaps in natural frequency dispersive media (FDM) are caused by electromagnetic coupling to elementary excitations (excitons, optical phonons, etc.) of the media [16,17]. In this paper we also investigate Raman scattering from a three-level atom embedded in a FDM. We demonstrate that the condition for occurrence of a photon-atom bound state is much more stringent in the FDM case than in the PBG case. We also show that the spectral splitting observed in the PBG case (when one of the transition frequencies is near the upper band edge of the gap) is absent in the FDM case. These differences are explained by considering the near band-edge behavior of the density of photon states in the two different materials.

II. MODEL HAMILTONIAN

Consider a physical system consisting of a single three-level atom embedded in a PBG material (or a FDM). Let $|0\rangle$ denote the ground level of the atom and let $|1\rangle$ and $|2\rangle$ be the two excited levels (see Fig. 1). Normalization and orthogonality require that $\langle i|j\rangle = \delta_{ij}$, where δ_{ij} is the Krönecker delta. We designate the energy of an atomic level $|i\rangle$

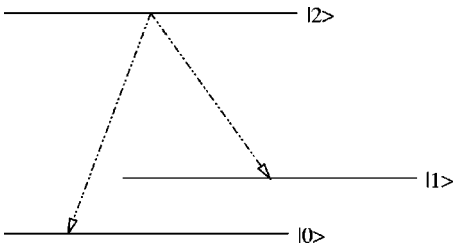

FIG. 1. Schematic representations of a three-level system in the Λ configuration. Dashed lines with arrows denote dipole allowed transitions. In the Λ configuration, levels $|1\rangle$ and $|0\rangle$ are of the same symmetry and the transition $|1\rangle \rightarrow |0\rangle$ is not dipole allowed.

by $\hbar\omega_i$ and the frequency separation between levels $|i\rangle$ and $|j\rangle$ by $\omega_{ij}=\omega_i-\omega_j$. Transitions between the atomic levels can be described using the atomic operators $\sigma_{ij}=|i\rangle\langle j|$ with the property $\sigma_{ij}|k\rangle=\delta_{jk}|i\rangle$ from which the commutation relation

$$[\sigma_{ij},\sigma_{lk}]=\delta_{jl}\sigma_{ik}-\delta_{ik}\sigma_{lj} \tag{1}$$

can readily be obtained. The three-level atom is assumed to be in the Λ configuration where the upper most atomic level $|2\rangle$ is dipole coupled to the lower levels $|1\rangle$ and $|0\rangle$ by radiation modes (photon reservoir) in a three-dimensional PBG or FDM. The transition $|1\rangle \rightarrow |0\rangle$ is dipole forbidden.

We consider the resonance Raman scattering of a laser pulse of frequency $\omega_L=\omega_{20}$ from the three-level atom. The radiation scattered by the atom consists of Stokes and Raleigh components with frequencies $\omega_S=\omega_L-\omega$ and $\omega_R=\omega_L$, respectively. Accordingly, we divide the photon reservoir into two parts, one consisting of the Raleigh modes (identified by the subscript R) and the other consisting of the Stokes modes (identified by the subscript S).

Our consideration in this paper is restricted to the case of isotropic photonic band gaps where the band edge is associated with a sphere $|\mathbf{k}|=k_0$ in k space (spherical Brillouin zone). The spectrum of elementary electromagnetic excitations in such an isotropic PBG has the form shown in the inset of Fig. 2. Due to the spherical symmetry of the problem, it is convenient to use the spherical harmonic representation for dynamical variable of the system. In this representation, the model Hamiltonian H of our atom-field system can be written as [14]

$$\begin{aligned} H=&\sum_{j=1,2}\omega_{j0}\sigma_{jj}+\sum_{\alpha=R,S}\int_{C_\alpha}\frac{d\omega}{2\pi}\omega a_\alpha^\dagger(\omega)a_\alpha(\omega)\\ &-\int_{C_R}\frac{d\omega}{2\pi}\sqrt{z_{20}(\omega)}[a_R^\dagger(\omega)\sigma_{02}+\sigma_{20}a_R(\omega)]\\ &-\int_{C_S}\frac{d\omega}{2\pi}\sqrt{z_{21}(\omega)}[a_S^\dagger(\omega)\sigma_{12}+\sigma_{21}a_S(\omega)], \end{aligned} \tag{2}$$

where we choose units in which $\hbar=c=1$. The first term in Eq. (2) represents the Hamiltonian of the bare atom, taking the zero of energy to be at level $|0\rangle$ so that $\omega_0=0$. The second term represents the Hamiltonian of the photon reservoir which is decomposed into Rayleigh and Stokes components. Associated with the Rayleigh and Stokes modes are the radiation field annihilation and creation operators, $a_\alpha(\omega)$ and $a_\alpha^\dagger(\omega)$, obeying the commutation rules

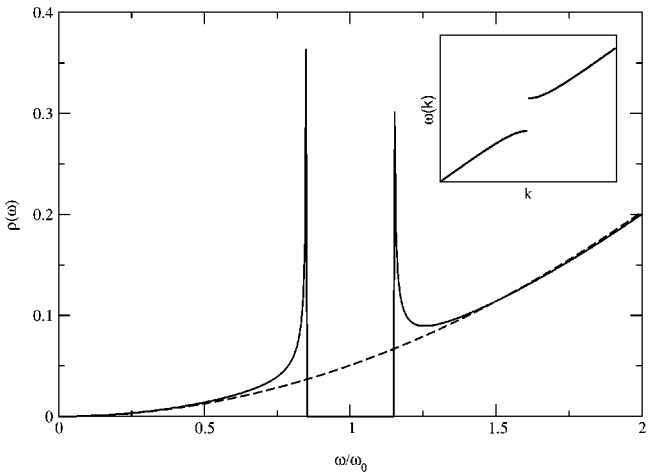

FIG. 2. The photon density-of-states $\rho(\omega)$ in a PBG material described by the isotropic dispersion relation (54). The dashed curve represents the free space density of photon states, $\rho(\omega)=\omega^2/2\pi$. For isotropic PBG, $\rho(\omega)$ exhibits singularities at both band edges behaving like $\rho(\omega)\sim(\omega_v-\omega)^{-1/2}$ for $\omega<\omega_v$, and like $\rho(\omega)\sim(\omega-\omega_c)^{-1/2}$ for $\omega>\omega_c$. Far from the band edges, $\rho(\omega)$ is essentially the same as that of free space, as expected. A typical isotropic dispersion relation for a PBG material is shown in the inset.

$$[a_\alpha(\omega),a_{\alpha'}^\dagger(\omega')]=2\pi\delta_{\alpha\alpha'}\delta(\omega-\omega'). \tag{3}$$

We assume that the Rayleigh and Stokes components are well separated in frequency so that their corresponding operators commute. We also assume that atomic operators σ_{ij} commute with the field operators $a_\alpha(\omega)$ and $a_\alpha^\dagger(\omega)$ for the quantized Stokes and Rayleigh modes.

The last two terms in Eq. (2) represent interaction Hamiltonians. The third term describes the interaction between the atom and the Rayleigh part of the photon reservoir, whereas the fourth term describes the interaction between the atom and the Stokes part of the photon reservoir. These interaction Hamiltonians are written in the electric dipole approximation. They are also written in the rotating wave approximation [18] in which virtual processes of excitation (de-excitation) of the atom with simultaneous creation (annihilation) of a photon [i.e., terms of the form $a_R^\dagger(\omega)\sigma_{20}$ and $a_R(\omega)\sigma_{02}$] are neglected.

As shown in the inset of Fig. 2, the photon frequency varies from zero to ω_v within the lower branch and from ω_c to $+\infty$ within the upper branch, where ω_v and ω_c are the lower and upper band-edge frequencies, respectively. The gap width is $\Delta\equiv\omega_c-\omega_v$ and the gap to midgap ratio is $r\equiv\Delta/\omega_o$, where ω_o is the midgap frequency. We denote by G the frequency range spanning the gap:

$$G\equiv(\omega_v,\omega_c). \tag{4}$$

Thus, the integration contour C_α in Eq. (2) are subsets of the full contour

$$C=[0,\omega_v]\cup[\omega_c,\infty)=[0,\infty)-G. \tag{5}$$

Within the band gap, there are no propagating photon modes in any direction in space so that the density of photon modes

$$\rho(\omega)=0, \quad \omega\in G. \tag{6}$$

In the Hamiltonian (2), the frequency dependent coupling constant $\sqrt{z_{2j}(\omega)}$, between the atomic transition $|2\rangle\rightarrow|j\rangle$ and the corresponding photon reservoir is given by

$$z_{2j}(\omega)=\gamma_{2j}(\omega)z(\omega), \tag{7}$$

where $\gamma_{2j}(\omega)$ represents the coupling constant of the atomic transition $|2\rangle\rightarrow|j\rangle$ with the free space photon reservoir [that is, $\gamma_{2j}(\omega)$ gives the free space spontaneous emission rate for the transition $|2\rangle\rightarrow|j\rangle$] and

$$z(\omega)=\left(\frac{d\omega}{dk}\right)^{-1} \tag{8}$$

is the ''atomic form factor.'' As shown in Appendix A, $z(\omega)$ can be expressed in terms of the photon density-of-state $\rho(\omega)$ as

$$z(\omega)\equiv\frac{2\pi^2\rho(\omega)}{k^2(\omega)}. \tag{9}$$

Clearly, $z(\omega)$ is proportional to $\rho(\omega)$ and vanishes wherever $\rho(\omega)$ vanishes, such as within a photonic band gap:

$$z(\omega)=0, \quad \omega\in G. \tag{10}$$

In the resonance approximation we replace $\gamma_{2j}(\omega)$ in Eq. (7) by the constant value

$$\gamma_{2j}=\tfrac{4}{3}\omega_{2j}^3 d_{2j}^2, \tag{11}$$

where d_{2j} represents the magnitude of the dipole moment for the transition $|2\rangle\rightarrow|j\rangle$ and we extend the contours C_α in Eq. (2) to

$$C_\infty=(-\infty,\omega_v]\cup[\omega_c,\infty)=(-\infty,\infty)-G. \tag{12}$$

The operator for the number of excitations of our model system (atom plus radiation field)

$$N=\sigma_{22}+\sum_{\alpha=R,S}\int_C\frac{d\omega}{2\pi}a_\alpha^\dagger(\omega)a_\alpha(\omega) \tag{13}$$

commutes with the model Hamiltonian, $[N,H]=0$. Thus all eigenstates of the model can be classified with respect to the number of excitations or eigenvalues of the operator N and we can separately study the sectors of Hilbert space containing different number of excitations. In this paper we deal only with the one-excitation problem. Two-excitation problems are discussed elsewhere [19].

III. ONE-PARTICLE PROBLEM

A. One-particle eigenstates

We look for one-particle eigenstates of the number operator N in the form

$$|\Psi_1\rangle=\left\{\xi\sigma_{20}+\int_C\frac{d\omega}{2\pi}[\psi_S(\omega)a_S^\dagger(\omega)\sigma_{10}+\psi_R(\omega)a_R^\dagger(\omega)]\right\}|vac\rangle, \tag{14}$$

where the vacuum state $|vac\rangle$ is defined as the state in which the atom is in the ground state $|0\rangle$ and there is no photon in the system so that $a_\alpha(\omega)|vac\rangle=0$. The amplitude ξ gives the probability of finding the atom in the excited state $|2\rangle$ and both photon reservoirs in the vacuum state. The operator product $a_S^\dagger(\omega)\sigma_{10}$ acting on the vacuum state $|vac\rangle$ excites the atom to the upper level $|1\rangle$ while creating a Stokes photon of frequency ω, and $\psi_S(\omega)$ gives the amplitude for this process. On the other hand, $a_R^\dagger(\omega)$ acting on $|vac\rangle$ creates a Rayleigh photon of frequency ω but leaves the atom in the ground state $|0\rangle$ and $\psi_R(\omega)$ gives the amplitude for this process.

The state $|\Psi_1\rangle$ is a one-particle eigenstate of the number operator $N|\Psi_1\rangle=|\Psi_1\rangle$. Now let $|\Psi_1\rangle$ also be an eigenstate of the Hamiltonian (2) with the eigenvalue ϵ:

$$H|\Psi_1\rangle=\epsilon|\Psi_1\rangle. \tag{15}$$

Projecting this time-independent Schrödinger equation onto $a_R^\dagger(\omega)|vac\rangle$, $a_S^\dagger(\omega)\sigma_{10}|vac\rangle$, and $\sigma_{20}|vac\rangle$, respectively, we obtain

$$(\omega-\epsilon)\psi_R(\omega|\epsilon)=\sqrt{z_{20}(\omega)}\xi(\epsilon), \tag{16a}$$

$$(\omega-\epsilon+\omega_{10})\psi_S(\omega|\epsilon)=\sqrt{z_{21}(\omega)}\xi(\epsilon), \tag{16b}$$

$$(\omega_{20}-\epsilon)\xi(\epsilon)=\int_{C_\infty}\frac{d\omega}{2\pi}[\sqrt{z_{20}(\omega)}\psi_R(\omega|\epsilon)+\sqrt{z_{21}(\omega)}\psi_S(\omega|\epsilon)]. \tag{16c}$$

The general solutions of Eqs. (16a) and (16b) are

$$\psi_R(\omega|\epsilon)=2\pi\chi_R(\epsilon)\delta(\omega-\epsilon)+\frac{\sqrt{z_{20}(\omega)}}{\omega-\epsilon-i0}\xi(\epsilon), \tag{17a}$$

$$\psi_S(\omega|\epsilon)=2\pi\chi_S(\epsilon)\delta(\omega-\epsilon+\omega_{10})+\frac{\sqrt{z_{21}(\omega)}}{\omega-\epsilon+\omega_{10}-i0}\xi(\epsilon), \tag{17b}$$

where $\chi_R(\epsilon)$ and $\chi_S(\epsilon)$ are as yet undetermined arbitrary functions that can be fixed by specifying asymptotic (boundary) values for ψ_R and ψ_S. In Eqs. (17a) and (17b), the eigenvalue ϵ is made slightly complex by adding a small positive imaginary part $(i0)$ to it. This is a standard procedure in scattering theory [20] to get around the singularities associated with both $1/(\omega-\epsilon)$ and $1/(\omega-\epsilon+\omega_{10})$. The

choice of sign before the small imaginary part $i0$ depends on the system's initial configuration. The minus sign corresponds (as in our case) to an initially incident (incoming) photon.

B. Self-energy

Substituting Eqs. (17a) and (17b) into Eq. (16) to eliminate the wave functions $\psi_\alpha(\omega|\epsilon)$, we obtain

$$[\omega_{20}-\epsilon-\Sigma(\epsilon)]\xi(\epsilon)=\sqrt{z_{20}(\epsilon)}\chi_R(\epsilon)+\sqrt{z_{21}(\epsilon-\omega_{10})}\chi_S(\epsilon), \tag{18}$$

where

$$\Sigma(\epsilon)=\int_{C_\infty}\frac{d\omega}{2\pi}\left[\frac{z_{20}(\omega)}{\omega-\epsilon-i0}+\frac{z_{21}(\omega)}{\omega-\epsilon+\omega_{21}-i0}\right] \tag{19}$$

is referred to as the self-energy of the system. Using the identity

$$\lim_{\eta\to 0}\left(\frac{1}{x\pm i\eta}\right)=P\left(\frac{1}{x}\right)\mp i\pi\delta(x), \tag{20}$$

where P denotes the Cauchy principal [21], we can decompose the self-energy $\Sigma(\epsilon)$ into real and imaginary parts as

$$\Sigma(\epsilon)=\Sigma'(\epsilon)+i\Sigma''(\epsilon), \tag{21}$$

where

$$\Sigma'(\epsilon)=\gamma_{20}P\int_{C_\infty}\frac{d\omega}{2\pi}\frac{z(\omega)}{\omega-\epsilon}+\gamma_{21}P\int_{C_\infty}\frac{d\omega}{2\pi}\frac{z(\omega)}{\omega-\epsilon+\omega_{10}}, \tag{22a}$$

$$\Sigma''(\epsilon)=\frac{1}{2}[\gamma_{20}z(\epsilon)+\gamma_{21}z(\epsilon-\omega_{10})], \tag{22b}$$

and we have used Eq. (7) in the resonance approximation.

The real part $\Sigma'(\epsilon)$ gives the energy shift of level $|2\rangle$ due to the atom-field interaction. Assuming that the main contribution to $\Sigma'(\epsilon)$ comes from the region near the transition frequency ω_{20}, we can evaluate $\Sigma'(\epsilon)$ at $\epsilon=\omega_{20}$ and incorporate this value in the definition of the energy of level $|2\rangle$. Accordingly, we introduce

$$\nu_{20}=\omega_{20}-\Sigma'(\omega_{20}) \tag{23}$$

as the new transition frequency when the atom is in the medium. The first integral on the right-hand side of Eq. (22a) is of the order γ_{21} except in the neighborhood of $\omega\sim\epsilon$ or in regions where $z(\omega)$ [or equivalently the photon density-of-states $\rho(\omega)$] is very large. On the other hand, the decay rate γ_{20} is smaller than optical transition frequency ω_{20} by at least six orders of magnitude ($\gamma_{20}\sim 10^8$ s^{-1} whereas $\omega_{20}\sim 10^{15}$ s^{-1}). Thus, whatever the value of the first integral, it cannot offset the smallness of γ_{20} and we can safely assume that the first term on the right-hand side of Eq. (22a) is very small compared to an optical transition frequency. The same applies for the second term. It follows that $\Sigma'(\omega_{20})\ll\omega_{20}$. From Eq. (22a) we obtain

$$\frac{d\Sigma'(\epsilon)}{d\epsilon}=P\int_C\frac{d\omega}{2\pi}\left[\frac{\gamma_{20}z(\omega)}{(\omega-\epsilon)^2}+\frac{\gamma_{21}z(\omega)}{(\omega-\epsilon+\omega_{10})^2}\right]>0, \tag{24}$$

which indicates that $\Sigma'(\epsilon)$ is a monotonically increasing function of ϵ.

The imaginary part $\Sigma''(\epsilon)$ of the self-energy gives the decay rate of the upper level $|2\rangle$. In other words, the atom decays from the excited state $|2\rangle$ with a lifetime of $1/\Sigma''(\epsilon)$. From Eqs. (9) and (22b) we see that

$$\Sigma''(\epsilon)\sim\frac{\gamma_{20}}{2}\rho(\epsilon)+\frac{\gamma_{21}}{2}\rho(\epsilon-\omega_{10}). \tag{25}$$

Like the real part $\Sigma'(\epsilon)$, the imaginary part $\Sigma''(\epsilon)$ is proportional to the decay rates γ_{2j} and is very small except in regions where the local photon density-of-states is very large. However, unlike $\Sigma'(\epsilon)$, $\Sigma''(\epsilon)$ cannot possibly be neglected since this would lead to infinite lifetime for the excited atomic state $|2\rangle$.

The electromagnetic vacuum is characterized by the dispersion relation $\omega(k)=k$. For such a dispersion relation, Eqs. (7) and (8) give $z_{2j}(\omega)=\gamma_{2j}(\omega)$ for the coupling constant which, in the resonance approximation, is replaced by the constant value given by Eq. (11). Moreover, since there is no gap in the free space photon density-of-states, the contour C_∞ in Eq. (22a) extends over the entire real axis, $C=(-\infty,\infty)$. Equations (22a) and (22b) then give

$$\Sigma'(\epsilon)=P\int_{-\infty}^{\infty}\frac{d\omega}{2\pi}\left(\frac{\gamma_{20}}{\omega-\epsilon}+\frac{\gamma_{21}}{\omega-\epsilon+\omega_{10}}\right)=0, \tag{26a}$$

$$\Sigma''(\epsilon)=(\gamma_{20}+\gamma_{21})/2 \tag{26b}$$

for the real and imaginary parts of the self-energy in free space. Thus the real part of the free space self-energy is identically zero, while the imaginary part is half the sum of the decay rates for the two allowed decay channels, $|2\rangle\to|0\rangle$ and $|2\rangle\to|1\rangle$. Note that the principal part in Eq. (26a) vanishes because we have extended the lower limit of integration to $-\infty$ by applying the resonance approximation. Had we not done so, the principal part would have given rise to a nonzero contribution (in fact, divergent contribution, which has to be corrected by introducing a cutoff [22,23] on the energy of photons) which is associated with the Lamb shift of the atomic levels. Even in this case, however, we can set the principal value term to zero by assuming that the Lamb shifts are incorporated into the definition of our state energies.

C. Auxiliary space

The amplitude functions $\psi_\alpha(\omega|\epsilon)$ can be cast into a more familiar form by introducing a τ space [15], which is auxiliary to the ω space. This auxiliary space is defined by the Fourier transforms

$$a_\alpha(\omega)=\int_{-\infty}^{\infty}d\tau a_\alpha(\tau)e^{-i\omega\tau}, \tag{27a}$$

$$\psi_\alpha(\omega|\epsilon)=\int_{-\infty}^{\infty}d\tau\psi_\alpha(\tau|\epsilon)e^{-i\omega\tau}. \tag{27b}$$

The inverse Fourier transforms are given by

$$a_\alpha(\tau)=\frac{1}{2\pi}\int_{-\infty}^{\infty}d\omega a_\alpha(\omega)e^{i\omega\tau}, \tag{28a}$$

$$\psi_\alpha(\tau|\epsilon)=\frac{1}{2\pi}\int_{-\infty}^{\infty}d\omega\psi_\alpha(\omega|\epsilon)e^{i\omega\tau}. \tag{28b}$$

Taking the Fourier transforms of Eqs. (17a) and (17b) we obtain

$$\psi_R(\tau|\epsilon)=[\chi_R(\epsilon)+iq_R(\epsilon)\Theta(\tau)]e^{i\epsilon\tau}, \tag{29a}$$

$$\psi_S(\tau|\epsilon)=[\chi_S(\epsilon)+iq_(\epsilon)\Theta(\tau)e^{i(\epsilon-\omega_{10})\tau}, \tag{29b}$$

where

$$q_R(\epsilon)=\sqrt{z_{20}(\epsilon)}\xi(\epsilon), \tag{30a}$$

$$q_S(\epsilon)=\sqrt{z_{21}(\epsilon-\omega_{10})}\xi(\epsilon), \tag{30b}$$

and $\xi(\epsilon)$ is given by Eq. (18):

$$\xi(\epsilon)=\frac{\sqrt{z_{20}(\epsilon)}\chi_R(\epsilon)+\sqrt{z_{21}(\epsilon-\omega_{10})}\chi_S(\epsilon)}{\omega_{20}-\epsilon-\Sigma(\epsilon)}. \tag{31}$$

In Eqs. (29a) and (29b) $\Theta(\tau)$ represents the unit step function defined by

$$\Theta(\tau)=\begin{cases}1 & \text{for } \tau>0\\ 0 & \text{for } \tau<0.\end{cases} \tag{32}$$

From Eqs. (29a) and (29b) we identify $iq_R(\epsilon)$ and $iq_S(\epsilon)$ as the scattering amplitudes for the Rayleigh and Stokes modes, respectively. The scattering cross sections, i.e., the probability for an incident photon of frequency ω to be scattered in the Rayleigh or the Stokes channel are given by

$$\sigma_R(\omega)\propto|iq_R(\omega)|^2=\gamma_{20}z(\omega)|\xi(\omega)|^2, \tag{33a}$$

$$\sigma_S(\omega)\propto|iq_S(\omega)|^2=\gamma_{21}z(\omega-\omega_{10})|\xi(\omega)|^2, \tag{33b}$$

where we have used Eq. (7) in the resonance approximation. Using Eq. (9) in Eq. (33a) we notice that

$$\sigma_R(\omega)\propto\rho(\omega),\quad \sigma_S(\omega)\propto\rho(\omega-\omega_{10}) \tag{34}$$

D. Discrete mode

Equations (17a) and (17b), together with a choice of values for the arbitrary functions $\chi_R(\epsilon)$ and $\chi_S(\epsilon)$ [depending on the boundary conditions for $\psi_R(\omega|\epsilon)$ and $\psi_S(\omega|\epsilon)$] completely determine the one-particle spectrum of the system. In this section we look for a discrete mode of the system with frequency ϵ_d such that both ϵ_d and $\epsilon_d-\omega_{10}$ lie within the frequency gap G. This requires that

$$\epsilon_d\in G', \tag{35}$$

where

$$G'\equiv(\omega_v+\omega_{10},\omega_c) \tag{36}$$

is a subinterval of $G=(\omega_v,\omega_c)$. Thus for both ϵ_d and $\epsilon_d-\omega_{10}$ to lie within the gap G, we must have $\omega_v+\omega_{10}<\omega_c$ or

$$\omega_{10}<\omega_c-\omega_v=\Delta. \tag{37}$$

In other words, the transition frequency $\omega_{10}=\omega_{20}-\omega_{21}$ must be less than the width of the gap. When both ϵ_d and $\epsilon_d-\omega_{10}$ lie within the gap, Eq. (10) shows that both $z(\epsilon_d)$ and $z(\epsilon_d-\omega_{10})$ are zero so that, according to Eq. (22b), the imaginary part $\Sigma''(\epsilon)$ of the self-energy is also zero:

$$\Sigma''(\epsilon_d)=0,\quad \epsilon_d\in G'. \tag{38}$$

Within the band gap, single-photon spontaneous emission is completely inhibited [5]. When both ϵ_d and $\epsilon_d-\omega_{10}$ lie within the gap, we have $\omega\neq\epsilon_d$ and $\omega\neq\epsilon_d-\omega_{10}$ and the first terms on the right-hand side of both Eqs. (17a) and (17b) do not contribute to $\psi_R(\omega|\epsilon_d)$ and $\psi_S(\omega|\epsilon_d)$, respectively. Therefore, when condition (35) is satisfied, we can choose

$$\chi_R(\epsilon_d)=\chi_S(\epsilon_d)=0,\quad \epsilon_d\in G'. \tag{39}$$

This choice can then be used in Eqs. (17a), (17b), and (18) to obtain

$$\psi_R(\omega|\epsilon_d)=\frac{\sqrt{z_{20}(\omega)}}{\omega-\epsilon_d}\xi(\epsilon_d), \tag{40a}$$

$$\psi_S(\omega|\epsilon_d)=\frac{\sqrt{z_{21}(\omega)}}{\omega-\epsilon_d+\omega_{10}}\xi(\epsilon_d), \tag{40b}$$

and

$$[\omega_{20}-\epsilon_d-\Sigma'(\epsilon_d)]\xi(\epsilon_d)=0. \tag{41}$$

In Eq. (41) we have used Eq. (38) to replace $\Sigma(\epsilon_d)$ by the real part $\Sigma'(\epsilon_d)$.

Apart from the trivial solution $\xi(\epsilon_d)=0$, Eq. (41) has a nontrivial solution $\xi(\epsilon_d)\neq0$ provided that an eigenenergy ϵ_d is found such that

$$\omega_{20}-\epsilon_d-\Sigma'(\epsilon_d)=0,\quad \epsilon_d\in G'. \tag{42}$$

Since, $\Sigma'(\epsilon)$ is a monotonically increasing function of ϵ [see Eq. (24)], Eq. (42) can have only one root $\epsilon=\epsilon_d$ given by the intersection of the curve $\Sigma'(\epsilon)$ with the straight line $\omega_{20}-\epsilon$. Clearly, a discrete bound state occurs only if the straight line $y(\epsilon)=\omega_{20}-\epsilon$ intersects the curve $\Sigma''(\epsilon)$ within the frequency range G' where, according to Eq. (38), $\Sigma''(\epsilon)=0$.

Substituting Eqs. (40a) and (40b) into Eq. (14), we find this discrete eigenstate of the system:

$$|\Psi_d\rangle=\xi(\epsilon_d)\left\{\sigma_{20}+\int_{C_\infty}\frac{d\omega}{2\pi}\left[\frac{\sqrt{z_{21}(\omega)}}{\omega-\epsilon_d+\omega_{10}}a_S^\dagger(\omega)\sigma_{10}+\frac{\sqrt{z_{20}(\omega)}}{\omega-\epsilon_d}a_R^\dagger(\omega)\right]|vac\rangle\right\}. \tag{43}$$

The function $\xi(\epsilon_d)$ is determined from the normalization condition $\langle\Psi_d|\Psi_d\rangle=1$. We obtain

$$|\xi(\epsilon_d)|^2=\left[1+\gamma_{20}\int_{C_\infty}\frac{d\omega}{2\pi}\frac{z(\omega)}{(\omega-\epsilon_d)^2}+\gamma_{21}\int_{C_\infty}\frac{d\omega}{2\pi}\frac{z(\omega)}{(\omega-\epsilon_d+\omega_{10})^2}\right]^{-1}. \quad (44)$$

When the system (atom + field) is in the discrete bound state $|\Psi_d\rangle$, the probability to find the atom in the excited state $|2\rangle$ is given by

$$P_2=|\xi(\epsilon_d)|^2. \quad (45)$$

The integrals in Eq. (44) are not principal value integrals since both ϵ_d and $\epsilon_d-\omega_{10}$ lie within the band gap G and therefore do not lie on the contour of integration C_∞. Thus

$$P_2\approx(1+\gamma_{20}+\gamma_{21})^{-1}\approx 1, \quad (46)$$

since $\gamma_{2j}\ll 1$. It follows that, when the system is in the photon-atom bound state $|\Psi_d\rangle$, the atom spends most of its time on the excited state $|2\rangle$. Once in a while, the atom drops to the lower state $|1\rangle$ by emitting a Stokes photon or to the ground state $|0\rangle$ by emitting a Rayleigh photon. However, the emitted photon is quickly re-absorbed by the atom, which is then re-excited to level $|2\rangle$.

The discrete mode (43) describes the three-level atom analog of the photon-atom bound state predicted by John and Wang [5] for a hydrogenic atom. In the present case there are two scattering channels, the elastic (Rayleigh) and the inelastic (Stokes or anti-Stokes) channels. A photon of frequency ω incident on an unexcited atom (atom on level $|0\rangle$) can be scattered in the Rayleigh channel preserving its frequency or in the Stokes channel, in which the atom is excited to level $|1\rangle$ and a Stokes photon of frequency $\omega_S=\omega-\omega_{10}$ is created. Alternately, the photon can be scattered from an excited atom on level $|1\rangle$ accompanied by the creation of an anti-Stokes photon of frequency $\omega_{AS}=\omega+\omega_{10}$ and the de-excitation of the atom to the ground level $|0\rangle$. Thus, in the three-level atom case, the radiation field is bound to the atom as a result of two-channel scattering, while the atom switches between levels $|0\rangle$ and $|1\rangle$ via the intermediate state $|2\rangle$.

According to Eq. (23) the solution of Eq. (42) can be written in terms of the shifted atomic transition frequency ν_{20} as $\epsilon_d=\nu_{20}$. There will be a discrete bound state only if ν_{20} (or roughly ω_{20}) lies in the frequency range between $\omega_v+\omega_{10}$ and ω_c. Moreover, condition (35) for the occurrence of a discrete bound state requires that the transition frequency $\omega_{10}=\omega_{20}-\omega_{21}$ be less than the width $\Delta=\omega_c-\omega_v$ of the gap. Thus for a discrete bound state to occur we must have $\omega_{21}\in G$ and $\omega_{20}\in G'$, where the frequency intervals G and G' are given by Eqs. (4) and (36), respectively. If, for instance, $\omega_{21}\notin G$, the bound state becomes quasi-bound. Its lifetime is determined by the possible irradiation of a photon of frequency ω_{21} in resonance with the escape channel $|2\rangle\rightarrow|1\rangle$.

E. Continuous spectrum

In this section we consider the case when the eigenvalue ϵ of Eq. (15) does not satisfy the discrete bound-state condition (35). This requires that $\epsilon\notin G'$. We investigate the scattering of a single incident laser photon of frequency ω from the three-level atom initially in the ground state. This initial condition (atom on level $|0\rangle$, a laser photon and no Stokes photon) determines the asymptotic (large distance) values of the amplitudes ψ_R and ψ_S uniquely and therefore fixes the functions $\chi_R(\epsilon)$ and $\chi_S(\epsilon)$ of Eqs. (17a) and (17b) to

$$\chi_R(\epsilon)=1, \quad \chi_S(\epsilon)=0. \quad (47)$$

Using this choice in Eq. (31) and substituting the result in Eqs. (33a) and (33b) we obtain

$$\sigma_R(\omega)\propto\frac{\gamma_{20}^2 z^2(\omega)}{[\omega_{20}-\omega-\Sigma'(\omega)]^2+[\Sigma''(\omega)]^2}, \quad (48a)$$

$$\sigma_S(\omega)\propto\frac{\gamma_{20}\gamma_{21}z(\omega)z(\omega-\omega_{10})}{[\omega_{20}-\omega-\Sigma'(\omega)]^2+[\Sigma''(\omega)]^2} \quad (48b)$$

as the scattering cross sections for the Rayleigh and Stokes channels. Here $\Sigma'(\omega)$ and $\Sigma''(\omega)$ are the real and imaginary parts of the self-energy given, respectively, by Eqs. (22a) and (22b). Equations (48a) and (48b) are written as functions of the incident laser photon frequency ω. The frequency of the scattered Rayleigh photons is $\omega_R=\omega$, whereas that of the Stokes photons is $\omega_S=\omega-\omega_{10}$.

Equations (48a) and (48b) show that scattering cross sections for the Rayleigh and Stokes components of the scattered light are strongly dependent on the atomic form factor $z(\omega)$ and on the self-energy $\Sigma(\omega)$. In the case of free space, $z(\omega)=1$ and the self energies are given by Eqs. (26a) and (26b). Using them in Eqs. (48a) and (48b) we obtain the free space scattering cross sections:

$$\sigma_R(\omega)\propto\frac{\gamma_{20}^2}{(\omega_{20}-\omega)^2+(\gamma_{20}+\gamma_{21})^2/4}, \quad (49a)$$

$$\sigma_S(\omega_S)\propto\frac{\gamma_{20}\gamma_{21}}{(\omega_{21}-\omega_S)^2+(\gamma_{20}+\gamma_{21})^2/4}. \quad (49b)$$

In Eq. (49b) we have used the relation $\omega_{21}=\omega_{20}-\omega_{10}$ to write $\sigma_S(\omega_S)$ as a function of the Stokes frequency $\omega_S=\omega-\omega_{10}$. Equations (49a) and (49b) represent two Lorentzian distributions of full width at half maximum (FWHM) $\Gamma=\gamma_{20}+\gamma_{21}$ peaked at the two transition frequencies ω_{20} and ω_{21}. The linewidth Γ is determined by the total lifetime of level $|2\rangle$, which can decay via either $|2\rangle\rightarrow|0\rangle$ (with decay rate γ_{20}) or $|2\rangle\rightarrow|1\rangle$ (with decay rate γ_{21}).

In a reservoir with a modified density of photon modes, the spectra of both the Rayleigh and the Stokes components of the scattered light will depart from a Lorentzian distribution in as much as the form factors $z(\omega)$ and the self-energy $\Sigma(\omega)$ in the medium deviate from their corresponding free space forms. In analyzing the continuous spectrum in such

modified reservoirs, we assume that the Rayleigh transition frequency ω_{20} lies far above the upper band edge ω_c and consider cases when the Stokes transition frequency ω_{21} lies in the neighborhood of ω_c. Thus the Rayleigh transition $|2\rangle \rightarrow |0\rangle$ can be considered to be occurring in a normal free space (Markovian reservoir) whereas the Stokes transition $|2\rangle \rightarrow |1\rangle$ occurs in a modified non-Markovian reservoir. Our main interest is to investigate effects on the Rayleigh spectrum due to the coupling of the Stokes transition $|2\rangle \rightarrow |1\rangle$ to the modified reservoir.

When ω_{20} lies far above the gap, the real and imaginary parts of the self-energy

$$\Sigma_R(\epsilon) = \gamma_{20} \int_{C_\infty} \frac{d\omega}{2\pi} \frac{z(\omega)}{\omega - \epsilon - i0} \tag{50}$$

corresponding to the Rayleigh component of the photon reservoir can be approximated by the free space values $\Sigma_R'(\epsilon) = 0$ and $\Sigma_R''(\epsilon) = i\gamma_{20}/2$. The real and imaginary parts of the total self-energy (19) will then be

$$\Sigma'(\epsilon) = \Sigma_S'(\epsilon), \tag{51a}$$

$$\Sigma''(\epsilon) = \gamma_{20}/2 + \Sigma_S''(\epsilon), \tag{51b}$$

where

$$\Sigma_S'(\epsilon) = \gamma_{21} P \int_{C_\infty} \frac{d\omega}{2\pi} \frac{z(\omega)}{\omega - \epsilon + \omega_{21}}, \tag{52a}$$

$$\Sigma_S''(\epsilon) = \frac{\gamma_{21}}{2} z(\epsilon - \omega_{10}) \tag{52b}$$

are the real and imaginary parts of the Stokes component. The Rayleigh scattering cross section becomes

$$\sigma_R(\omega) \propto \frac{\gamma_{20}^2 z^2(\omega)}{[\omega_{20} - \omega - \Sigma_S'(\omega)]^2 + [\gamma_{20} + 2\Sigma_S''(\omega)]^2/4}. \tag{53}$$

We investigate specific features of this cross section for the case of PBG and FDM separately in the following sections.

IV. SYSTEM IN A PBG MATERIAL

A. Model dispersion relation

We first consider the case where the three-level atom is embedded in an isotropic PBG. A simple model dispersion relation, which exhibits a gap in the photon density-of-states, is given by [8]

$$\omega(k) = \sqrt{k_0^2 + \gamma^2} \pm \sqrt{(k - k_0)^2 + \gamma^2}, \tag{54}$$

where $k = |\mathbf{k}|$ is the modulus of the wave vector, and k_0 and γ are parameters related to the periodic dielectric structure. The $+$ $(-)$ applies for the upper (lower) branch of the photon spectrum. Physically model (54) corresponds to placing an isotropic band gap of the form shown in the inset in Fig. 2 centered about the frequency $\omega_o = \sqrt{k_0^2 + \gamma^2}$, the lower and upper band-edge frequencies being $\omega_v = \omega_o - \gamma$ and $\omega_c = \omega_o + \gamma$. The width of the photonic band gap is $\Delta = \omega_c - \omega_v = 2\gamma$ and the gap to midgap ratio is $r \equiv \Delta/\omega_o = 2\gamma/\sqrt{k_0^2 + \gamma^2}$. In the context of photonic band-gap materials, the lower (upper) branch of the photon spectrum is more appropriately called the dielectric (air) band [24].

As shown in Appendix A, for a PBG material described by the dispersion relation (54) the atomic form factor $z(\omega)$ takes the form

$$z(\omega) = \begin{cases} \dfrac{|\omega - \omega_o|}{\sqrt{(\omega - \omega_v)(\omega - \omega_c)}}, & \omega \notin G \\ 0, & \omega \in G, \end{cases} \tag{55}$$

which, when used in Eq. (9), gives

$$\rho(\omega) = \begin{cases} \dfrac{|\omega - \omega_o|}{2\pi^2} \left[\dfrac{\omega^2 - 2\omega_o\omega + 2\omega_v\omega_c}{\sqrt{(\omega - \omega_v)(\omega - \omega_c)}} \pm 2\sqrt{\omega_v\omega_c} \right], \\ \qquad \omega \notin G \\ 0, \quad \omega \in G \end{cases} \tag{56}$$

for the density of photon modes. Here the $+(-)$ sign apply for $\omega > \omega_c$ $(\omega < \omega_v)$.

The density-of-states (56) is plotted in Fig. 2. For regions far removed from the band edges, $\rho(\omega)$ differs little from its free space value of $\omega^2/2\pi$, as expected. Near the band edges ω_v and ω_c, Eq. (56) shows that, $\rho(\omega)$ behaves as $\rho(\omega) \sim (\omega_v - \omega)^{-1/2}$ for $\omega < \omega_v$ and as $\rho(\omega) \sim (\omega - \omega_c)^{-1/2}$ for $\omega > \omega_c$, the square-root singularities being characteristic of a one-dimensional phase space [5]. These singularities are artifacts of the isotropic dispersion relation (54) which associates the band-edge wave vector with a sphere in k space, $|\mathbf{k}| = k_0$ (spherical Brillouin zone) and thereby artificially increases the true phase space available for photon propagation near the band edge. In a real three-dimensional dielectric crystal with an allowed point-group symmetry, the gap is highly anisotropic and the band edge is associated with a point $\mathbf{k} = \mathbf{k}_0$ (or a finite collection of symmetry related points) in k space [24], rather than with the entire sphere $|\mathbf{k}| = |\mathbf{k}_0|$. In this case the density of photon states is finite at the band-edge frequencies [25].

Using Eqs. (7) and (55) in Eq. (22b), we obtain the imaginary part $\Sigma''(\epsilon)$ of the self-energy for a PBG described by the isotropic dispersion relation (54). Likewise the real part $\Sigma'(\epsilon)$ is determined by using Eqs. (7) and (55) in Eq. (22a) and evaluating (numerically) the integral. For illustration, we consider an isotropic PBG with a gap to midgap ratio of $r = 15\%$, a ratio that can be achieved in practical PBG materials [25]. Thus, in units of the midgap frequency ω_o, the bandwidth is $\Delta = 0.15$, and the band-edge frequencies are at $\omega_v = 1 - r/2 = 0.925$ and $\omega_c = 1 + r/2 = 1.075$. In what follows, we fix the transition frequency to $\omega_{10} = \Delta/10 = 0.015\omega_o$. Then the frequency intervals G and G' are given by $G = (0.925, 1.075)$ and $G' = (0.94, 1.075)$. Also we choose $\gamma_{20} = \gamma_{21} = \omega_{10}/10$ for visualizaton purposes. In reality, $\gamma_{20} \ll \omega_{10}$ if ω_{10} is in the optical regime. However, as seen in Eqs. (22b) and (22a), the constants γ_{2j} appear only as

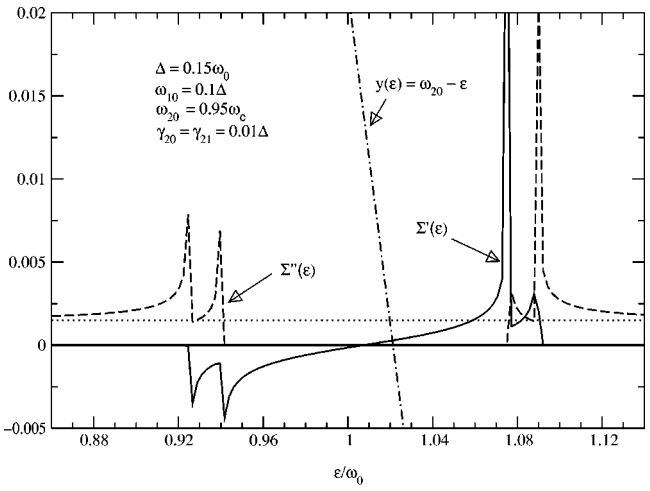

FIG. 3. The real part $\Sigma'(\epsilon)$ (solid curve) and the imaginary part $\Sigma''(\epsilon)$ (long-dashed curve) of the self-energy [Eqs. (22a) and (22b)] for a PBG material as functions of the scaled frequency ϵ/ω_o. Here, $r=15\%$, $\omega_v=0.925\omega_o$, $\omega_c=1.075\omega_o$, and the band-gap width is $\Delta=0.15\omega_o$. Also $\omega_{10}=\Delta/10=0.015\omega_o$ and $\omega_{20}=0.95\omega_c=1.012\omega_o$ so that $\omega_{20}\in G'$ and $\omega_{21}=1.006\omega_o\in G$. We also take $\gamma_{20}=\gamma_{21}=\Delta/100$. In the frequency range G' the imaginary part of the self-energy is identically zero whereas the real part is a monotonically increasing function of frequency. Both the real and imaginary parts of the self-energy exhibit singularities at the frequencies ω_v, $\omega_v+\omega_{10}$, ω_c, and $\omega_c+\omega_{10}$. The dotted curve represents the imaginary part of the free space self-energy given by $(\gamma_{20}+\gamma_{10}/2)$. The real part of the free space self-energy is identically zero [see Eq. (26b)]. The dot-dashed curve represents the straight line $y(\epsilon)=\omega_{20}-\epsilon$. This line intersects $\Sigma'(\epsilon)$ at $\epsilon\approx 1.02\omega_o\in G'$.

prefactors in the expressions for $\Sigma'(\epsilon)$ and $\Sigma''(\epsilon)$, and, therefore, their only effect is to change the scale of plots.

In Fig. 3 we plot the real part $\Sigma'(\epsilon)$ (solid curve) and the imaginary part $\Sigma''(\epsilon)$ (dashed curve) of the self-energy $\Sigma(\epsilon)$ as functions of the scaled frequency ϵ/ω_o for the case when both ω_{20} and ω_{21} lie inside the gap. The dotted curve represents the imaginary part of the free space self-energy given by Eq. (26b). The real part of the free space self-energy is identically zero [see Eq. (26a)]. According to Eq. (38), $\Sigma''(\epsilon)=0$ for $\epsilon\in G'=(0.94,1.075)$. Near the band edges, ω_v and ω_c, $\Sigma''(\epsilon)$ grows steadily from its free space value of unity, exhibiting singularities at $\omega_v=0.925$, $\omega_v+\omega_{10}=0.94$, $\omega_c=1.075$, and $\omega_c+\omega_{10}=1.09$. The singularities at the band-edge frequencies ω_v and ω_c are due to the term containing $z(\epsilon)$ [see Eqs. (22b) and (55)], whereas the singularities at the shifted frequencies $\omega_v+\omega_{10}$ and $\omega_c+\omega_{10}$ are due to the term containing $z(\epsilon-\omega_{10})$. Likewise, the real part $\Sigma'(\epsilon)$ of the self-energy is singular at the frequencies ω_v, $\omega_v+\omega_{10}$, ω_c and $\omega_c+\omega_{10}$. In the frequency range $\epsilon\in G'$, $\Sigma'(\epsilon)$ is a monotonically increasing function of ϵ. It is negative for $\epsilon<\epsilon_0$ and positive for $\epsilon>\epsilon_0$, where ϵ_0 denotes the zero of $\Sigma'(\epsilon)$. Far from the band gap, $\Sigma'(\epsilon)$ and $\Sigma''(\epsilon)$ are practically indistinguishable from their corresponding free space values, as expected.

B. Discrete modes in a PBG

In this section we investigate the photon-atom bound state in a PBG described by the isotropic dispersion relation (54). As discussed in Sec. III D, a discrete bound state can occur only when $\omega_{20}\in G'$ and $\omega_{21}\in G$, which in turn require ω_{10} to satisfy condition (37), i.e., ω_{10} should be less than the width $\Delta=\omega_c-\omega_v$ of the gap. The discrete bound state is given by the intersection of the straight line $y(\epsilon)=\omega_{20}-\epsilon$ with the curve $\Sigma'(\epsilon)$, provided that this intersection lies within the frequency range G' where $\Sigma''(\epsilon)=0$.

Using the same ω_{10} and PBG parameters as in Sec. IV A, we investigate the occurrence of a discrete bound state when ω_{20} (and hence ω_{21}) is varied with respect to the upper band edge ω_c. A discrete bound state occurs only if the curves $y(\epsilon)=\omega_{20}-\epsilon$ and $\Sigma'(\epsilon)$ intersect within the frequency range G'.

In Fig. 3 we plot the curves $\Sigma'(\epsilon)$ and $y(\epsilon)=\omega_{20}-\epsilon$ (as functions of the scaled frequency ϵ/ω_o) for the case when ω_{20} lies just below the upper band edge ($\omega_{20}=0.95\omega_c=1.021$) so that $\omega_{20}\in G'$ and $\omega_{21}=1.006\in G$. In this case we see that the straight line $y(\epsilon)=\omega_{20}-\epsilon$ intersects the curves $\Sigma'(\epsilon)$ at $\epsilon\approx 1.02\omega_o$, which lies within the frequency interval G'. This intersection point then represents the eigenvalue of a nondecaying photon atom bound state $|\Psi_d\rangle$ given by Eq. (43) with $\epsilon_d\approx 1.02$. As ω_{20} (and hence ω_{21}) is pushed further towards the upper band edge ω_c, the bound state is also pushed towards ω_c. When ω_{20} lies outside the gap, the straight line $y(\epsilon)$ no longer intersects the real part $\Sigma'(\epsilon)$ of the self-energy within the frequency range G', where $\Sigma''(\epsilon)=0$. This means that the solution of $\omega_{20}-\epsilon-\Sigma(\epsilon)=0$ has a nonzero imaginary part that serves to damp the system. Thus any initial population on the excited levels $|2\rangle$ and $|1\rangle$ will eventually decay to the ground level $|0\rangle$.

C. Continuous spectrum in PBG

We now analyze the spectrum equation (53) in the case of PBG. In what follows we fix ω_{20} to a value far above ω_c and plot the Rayleigh spectrum $\sigma_R(\omega)$ versus $\omega-\omega_{20}$ for various values of the Stokes transition frequency ω_{21}.

From Eqs. (10) and (53) we see that $\sigma_R(\omega)=0$ for $\omega\in G$. Thus in all plots of $\sigma_R(\omega)$ versus $\omega-\omega_{20}$, the Rayleigh spectrum will vanish completely in the ''spectral gap'' region $\omega-\omega_{20}\in G_s\equiv(\omega_v-\omega_{20},\omega_c-\omega_{20})$. From Eqs. (52b) and (55) we observe that the imaginary part $\Sigma_S''(\omega)$ of the self-energy exhibits square-root singularities at $\omega=\omega_v+\omega_{10}$ and $\omega=\omega_c+\omega_{10}$ leading to ''dark lines'' at $\omega-\omega_{20}=\omega_v-\omega_{21}$ and $\omega-\omega_{20}=\omega_c-\omega_{21}$ in $\sigma_R(\omega)$. These dark lines represent complete quenching of spontaneous emission at the respective frequencies and are separated exactly by the width $\Delta=\omega_c-\omega_v$ of the gap. They are shifted to higher frequencies when ω_{21} is decreased.

The dark lines here are artifacts of the isotopic dispersion relation (54), which leads to the atomic form factor $z(\omega)$ being singular at the band edges ω_v and ω_c as shown in Eq. (55). In real photonic crystals, the dispersion relation is anisotropic and $z(\omega)$ is not singular at the band edges [24]. Moreover, in realistic situations, relaxation processes in the medium should be taken into consideration [5,24]. One way to do this is to rewrite Eq. (55) in the form

$$z(\omega)=\begin{cases}\dfrac{|\omega-\omega_o|}{\sqrt{(\omega-\omega_v)(\omega-\omega_c)+\kappa^2}}, & \omega\notin G\\ 0, & \omega\in G,\end{cases}\tag{57}$$

where κ is a constant characteristic of the medium, introduced phenomenologically to account for relaxation processes. Thus in realistic situations, the Rayleigh spectrum will exhibit significant suppressions at $\omega=\omega_v+\omega_{10}$ and $\omega=\omega_c+\omega_{10}$ but not dark lines.

The dark lines at $\omega=\omega_v+\omega_{10}$ and $\omega=\omega_c+\omega_{10}$ split $\sigma_R(\omega)$ into triplets. These are ''band A,'' which lies to the left of $\omega_v+\omega_{10}$, ''band B,'' which lies between $\omega=\omega_v+\omega_{10}$ and $\omega=\omega_c+\omega_{10}$, and ''band C,'' which lies to the right of $\omega_c+\omega_{10}$. Band B measures the fractionalized steady-state atomic population on the excited state $|2\rangle$ due to the presence of the photonic band gap [6] and, therefore, can be used to experimentally probe this steady-state population. On the other hand, bands A and C measure the fraction of the excited-state population $|2\rangle$ that decays to the lower levels $|1\rangle$ and $|0\rangle$.

Spectral splitting was derived by John and Wang [5] in the effective-mass approximation to the dispersion relation (54) near the upper band edge ω_c, totally disregarding the effect of the lower band edge ω_v. One dark line and splitting into a doublet (bands B and C) was reported in the absence of an external field (vacuum Rabi splitting). The splitting was caused entirely by strong interaction between the atom and its own radiation field. More recently, dark lines have also been reported in Refs. [26,28].

For illustration, we consider an isotropic PBG with a gap to midgap ratio of $r=15\%$. In units of the midgap frequency ω_o, the bandwidth is $\Delta=0.15$ and the band edge frequencies are at $\omega_v=1-r/2=0.925$ and $\omega_c=1+r/2=1.075$ so that $G=(0.925,1.075)$. Also we choose $\gamma_{20}=\gamma_{21}=0.01\omega_{20}$ for the decay constants [27]. We fix the Rayleigh transition frequency to $\omega_{20}=1.2\omega_c=1.29$ so that ω_{20} is far from the band edge by more than the width Δ of the gap. Having fixed ω_{20}, we plot the Rayleigh spectrum $\sigma_R(\omega)$ versus $\omega-\omega_{20}$ for various values of the Stokes transition frequency ω_{21} in the neighborhood of the upper band edge ω_c. In all of these plots $\sigma_R(\omega)=0$ in the region $G_s=(-0.340,-0.215)$.

We are mainly interested in the behavior of $\sigma_R(\omega)$ in the neighborhood of the resonance $\omega-\omega_{20}=0$. In regions far from resonance, the value of $\sigma_R(\omega)$ is negligibly small compared its values in the resonance region. For instance, for our choice $\omega_{20}=1.2\omega_c$, the spectral gap $G_s=(-0.340,-0.215)$ lies far to the left the resonance region $\omega-\omega_{20}=0$ and is not shown in the plots.

First we consider the case when ω_{21} also lies far above the upper band edge. We take $\omega_{21}=1.15\omega_c=1.236$ so that ω_{21} is removed from the upper band edge ω_c by the width Δ of the gap. We then have $\omega_{10}=\omega_{20}-\omega_{21}=0.054$ and $\gamma_{20}=\gamma_{21}=\omega_{10}/10=0.0054$. Thus the dark lines of $\sigma_R(\omega)$ occur at $\omega=\omega_v+\omega_{10}=0.979$ and $\omega=\omega_c+\omega_{10}=1.129$ or at $\omega-\omega_{20}=-0.311$ and $\omega-\omega_{20}=-0.161$. The left-dark line lies within the spectral gap $G_s=(-0.340,-0.215)$. The spectrum corresponding to this choice of ω_{21} is shown by the dot-dashed curve in Fig. 4. The left- and right-dark lines occur far to the left of the resonance region $\omega-\omega_{20}=0$ and are not shown in the plot. From the plot we see that, for $\omega_{21}=1.15\omega_c$, $\sigma_R(\omega)$ practically consists only of band C, implying that all the population on the excited level $|2\rangle$ eventually decays to the lower levels $|1\rangle$ and $|0\rangle$. The plot also shows that band C is a Lorentzian with FWHM $\Gamma=\gamma_{20}+\gamma_{10}=0.011$. On the scale of this figure, the Rayleigh spectrum derived from Eq. (53) is indistinguishable from the free space spectrum [Eq. (49a)].

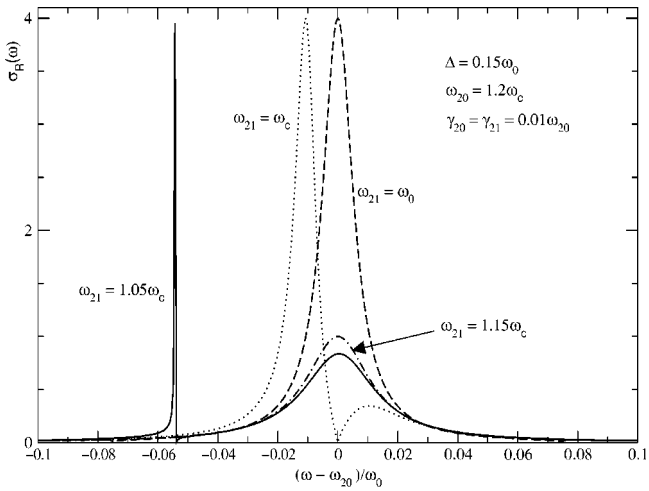

FIG. 4. The spectrum of spontaneous emission $\sigma_R(\omega)$ for the Rayleigh transition $|2\rangle\rightarrow|0\rangle$ in the case of PBG described by the isotropic dispersion relation (54). We take $r=15\%$, $\omega_{20}=1.2\omega_c$, and $\gamma_{20}=\gamma_{21}=0.01\omega_{20}$. Thus ω_{20} is removed from the band edge ω_c by more than the width of the gap. We plot $\sigma_R(\omega)$ for different values of the Stokes frequency ω_{21}, solid curve ($\omega_{21}=1.05\omega_c$), dotted curve ($\omega_{21}=\omega_c$), and dashed curve ($\omega_{21}=\omega_o$). The dot-dashed curve represents both Eqs. (53) and (49a) when $\omega_{21}=1.15\omega_c$. Thus the effect of the gap is negligible for transition frequencies removed from the band edge by at least the width Δ of the gap.

The effect of the band gap is negligible for transition frequencies removed from a band edge by at least the width Δ of the gap. This can be explained as follows. When ω_{21} lies far above the band edge ω_c, we can apply the Wigner-Weisskopf (WW) approximation for the Stokes channel and write $\Sigma_S'=0$, $\Sigma_S''=\gamma_{21}/2$. Since $z(\omega)=1$, Eq. (53) reduces to the free space equation (49a). Thus when both transition frequencies ω_{20} and ω_{21} lie far above the upper band edge ω_c, we expect the Rayleigh line to be a Lorentzian of FWHM $\Gamma=\gamma_{20}+\gamma_{10}$ centered at the frequency $\omega=\omega_{20}$, just like in free space. On the other hand, when ω_{21} is near the upper band edge, the density of electromagnetic modes changes rapidly in the vicinity of the atomic transition frequency ω_{21}, rendering the WW approximation to the self-energy $\Sigma_S(\epsilon)$ inadequate. In this case, we must perform an exact integration in Eq. (52a), which is then used in Eq. (53) to evaluate the spectrum $\sigma_R(\omega)$.

Next we consider the case when ω_{21} is close to the upper band edge ω_c. We take $\omega_{21}=1.05\omega_c=1.129$ so that $\omega_{10}=0.161$. Thus the left- and right-dark lines occur at $\omega-\omega_{20}=-0.204$ and $\omega-\omega_{20}=-0.054$, respectively. The

spectrum for this case is shown by the solid curve in Fig. 4. The left-dark line occurs far to the left of the resonance region $\omega-\omega_{20}=0$ and is not shown in the plot. For $\omega_{21}=1.05\omega_c$, $\sigma_R(\omega)$ practically consists only of two bands, bands B and C. The existence of band B shows that there is a fractionalized steady-state population on the excited level $|2\rangle$ even though ω_{20} lies outside the gap. The linewidth of band B is much smaller than the natural linewidth γ_{20} of the spontaneous transition $|2\rangle\rightarrow|0\rangle$ whereas the linewidth of band C is roughly the same as that of free space. When $\omega_{21}=1.05\omega_c$ most of the initial population on $|2\rangle$ decays to the lower levels and only a very small part is retained as a fractionalized steady-state population. As ω_{21} is pushed further towards ω_c, the dark lines are shifted to the right and the width of the band B increases, implying that more and more of the initial population is now retained as a fractionalized steady state-population. The dotted-curve in Fig. 4 represents the spectrum when ω_{21} coincides with the band edge, ω_c. In this case the left-dark line occurs at $\omega-\omega_{20}=-0.15$ and is not shown in the figure, whereas the right-dark line occurs at the resonance $\omega=\omega_{20}$.

Finally we consider the case when ω_{21} lies inside the gap. We take $\omega_{21}=\omega_o=1$, the midgap. Then $\omega_{10}=0.29$ and the left- and right-dark lines occur at $\omega-\omega_{20}=-0.075$ and $\omega-\omega_{20}=-0.075$, respectively, equidistant from the resonance frequency $\omega=\omega_{20}$. The spectrum for this case is shown by the dashed curve in Fig. 4. From the plot we see that by far the dominant contribution to $\sigma_R(\omega)$ comes from band B, implying that for $\omega_{21}=\omega_o$ most of the initial population on $|2\rangle$ is retained as a fractionalized steady-state population, and only a very small part decays to the lower levels.

V. SYSTEM IN A DISPERSIVE MEDIUM

In this section we briefly discuss the case when the three-level atom is embedded within a FDM. It is well known that a frequency gap for propagating electromagnetic modes exists in many natural dielectrics and semiconductors. Unlike in artificial PBG materials, where a suppression of the photon density-of-states over a narrow frequency range results from multiple photon scattering by a periodic array of scatterers, the gaps in dispersive media are caused by phonon coupling to elementary excitations of the media such as excitons and optical phonons [16,17]. The ''normal'' electromagnetic modes in frequency dispersive media are determined by the Maxwell equations with a frequency dependent dielectric permeability and are treated as ''photons in a medium,'' i.e., photons dressed by the interaction with a medium excitation. Their spectrum consists of two branches of allowed states separated by a gap in which propagating photon modes are completely forbidden.

A simple model dispersion relation for a frequency dispersive medium can be written as [15]

$$\omega_{\pm}(k)=\tfrac{1}{2}[(\Omega+k)\pm\sqrt{(\Omega-k)^2+4k\Delta}], \tag{58}$$

where Ω represents the longitudinal frequency of an optical phonon in the medium and Δ is the width of the frequency gap. The $+(-)$ sign applies for the upper (lower) branch of the photon spectrum. The dispersion relation (58) is plotted in the inset in Fig. 5. It exhibits an isotropic band gap centered about the frequency $\omega_o=\Omega-\Delta/2$. The lower and upper band-edge frequencies are $\omega_v=\Omega-\Delta$ and $\omega_c=\Omega$, respectively. The lower band edge occurs at $k\rightarrow\infty$, whereas the upper band edge occurs at $k=0$. The gap to midgap ratio is $r\equiv\Delta/\omega_o=\Delta/(\Omega-\Delta/2)$.

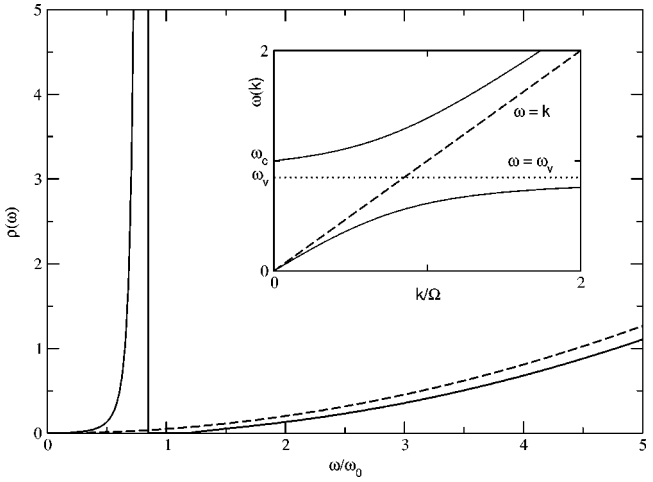

FIG. 5. The photon density-of-states in a dispersive medium described by the dispersion relation (58). The dashed curve represents the free space density of photon states. We see that $\rho(\omega)$ is highly singular at the lower band edge ω_v behaving like $\rho(\omega)\sim(\omega_v-\omega)^{-4}$, but is identically zero at the upper band edge, $\rho(\omega_c)=0$. This should be contrasted with the PBG case shown in Fig. 2 where $\rho(\omega)$ exhibits square-root singularities at both band edges. In the inset, the photon spectrum for a dispersive medium described by the dispersion relation (58) is shown.

As shown in Appendix A, the dispersion relation (58) gives

$$z(\omega)=\begin{cases}\dfrac{\omega^2-2\omega_v\omega+\omega_v\omega_c}{(\omega-\omega_v)^2+\kappa^2}, & \omega\notin G\\ 0, & \omega\in G,\end{cases} \tag{59}$$

for the form factor in a dispersive medium. Here we have added a phenomenological damping constant κ to account for relaxation processes in the medium. From Eq. (59) we see that at the upper band edge $z(\omega_c)=\omega_c/\Delta$, whereas near the lower band edge $z(\omega)\sim(\omega-\omega_v)^{-2}$. Unlike the PBG case, where $z(\omega)$ exhibits singularities at both band edges, $z(\omega)$ in a dispersive medium is singular only at the lower band edge ω_v and the square singularity here is much stronger than the square-root singularity of the isotropic PBG. From Eqs. (59) and (9) we obtain

$$\rho(\omega)=\begin{cases}\dfrac{\omega^2(\omega-\omega_c)^2}{2\pi^2}\left[\dfrac{\omega^2-2\omega_v\omega+\omega_v\omega_c}{(\omega-\omega_v)^4}\right], & \omega\notin G\\ 0, & \omega\in G\end{cases} \tag{60}$$

for the density of photon modes in a dispersive medium (see Appendix A).

The density-of-states 60 is plotted in Fig. (5). For regions far removed from the band gap, Eq. (60) shows that $\rho(\omega) \sim \omega^2/2\pi$, as expected. Near the lower band edge ω_v, $\rho(\omega)$ behaves as $\rho(\omega) \sim (\omega_v - \omega)^{-4}$ for $\omega < \omega_v$. On the other hand, near the upper band edge ω_c, $\rho(\omega)$ behaves as $\rho(\omega) \sim (\omega - \omega_c)^2$ for $\omega > \omega_c$. Thus $\rho(\omega)$ is highly singular at the lower band edge ω_v but is identically zero at the upper band edge, $\rho(\omega_c) = 0$. These near band-edge behaviors of $\rho(\omega)$ can easily be understood from the slope of the dispersion curve (58). For both the upper and lower branches we obtain

$$\left(\frac{d\omega}{dk}\right)_{\pm} = \frac{1}{2}\left[1 \pm \frac{(2\Delta - \Omega) + k}{\sqrt{(\Omega - k)^2 + 4\Delta k}}\right], \tag{61}$$

where the $+(-)$ sign applies for the upper(lower) branch. For $k \to \infty$, where the lower band edge occurs, we have $(d\omega/dk)_- \to 0$, which means that $\rho(\omega)$ is singular at ω_v. On the other hand at $k = 0$, where the upper band edge occurs, $(d\omega/dk)_+ = \Delta/\Omega$, which means that the group velocity is finite at the upper band edge ω_c (unless the width Δ of the gap is zero). The photon density-of-states, which behaves as $\rho \sim k/(d\omega/dk)_+$ [see Eq. (A5)] will then be zero at ω_c, since $k = 0$ there. The strong singularity of $\rho(\omega)$ at the lower band edge can be explained by the fact that we have allowed the wave vector $k \to \infty$ while, in reality, only wave vectors within the first Brillouin zone are relevant. This unrealistic singularity in the photon density-of-states is removed when we take relaxation processes in the medium into account.

Using Eq. (59) in Eq. (22b), we obtain the imaginary part $\Sigma''(\epsilon)$ of the self-energy for a dispersive medium described by the isotropic dispersion relation (58). Likewise, the real part $\Sigma'(\epsilon)$ is determined by substituting Eq. (59) into Eq. (22a) and evaluating (numerically) the integral. Both the real and imaginary parts of the self-energy are plotted in Fig. 6, where we choose $r = 15\%$, $\omega_{10} = \Delta/10$, $\omega_{20} = 0.95\omega_c$, and $\gamma_{20} = \gamma_{21} = \Delta/100$. The frequency intervals G and G' are given by (0.925,1.075) and (0.95,1.075), respectively. According to Eq. (38), $\Sigma''(\epsilon) = 0$ for $\epsilon \in G'$ and, according to Eqs. (22b) and (59), $\Sigma''(\epsilon)$ exhibits singularities at $\omega_v = 0.925$ and $\omega_v + \omega_{10} = 0.94$. Likewise, the real part $\Sigma'(\epsilon)$ is singular at ω_v and at $\omega_v + \omega_{10}$. In the frequency range $(\omega_v, \omega_v + \omega_{10})$, $\Sigma'(\epsilon)$ monotonically increases form $-\infty$ to $+\infty$ whereas outside this range $\Sigma'(\epsilon)$ asymptotically approaches the free space value of zero.

The differences between a PBG and a FDM described by the isotropic dispersion relations (54) and (58), respectively, can be observed by contrasting Figs. 3 and 6. In the PBG case, both $\Sigma'(\epsilon)$ and $\Sigma''(\epsilon)$ are singular at ω_v, ω_c, $\omega_v + \omega_{10}$, and $\omega_c + \omega_{10}$. In the FDM case, however, $\Sigma'(\epsilon)$ and $\Sigma''(\epsilon)$ are not singular at ω_c and $\omega_c + \omega_{10}$ but rather exhibit relatively large values (compared to the free space case) at these frequencies. In both the PBG and FDM cases $\Sigma''(\epsilon) = 0$ for $\epsilon \in G' = (0.94,1.075)$. However, in this frequency range, the real part $\Sigma'(\epsilon)$ behaves differently in the FDM from the PBG case. As we traverse G' from left to right (i.e., from $\epsilon = 0.94$ to $\epsilon = 1.075$), in the PBG case, $\Sigma'(\epsilon)$ monotonically increases from a very large negative value to a very large positive value passing through the free space value of

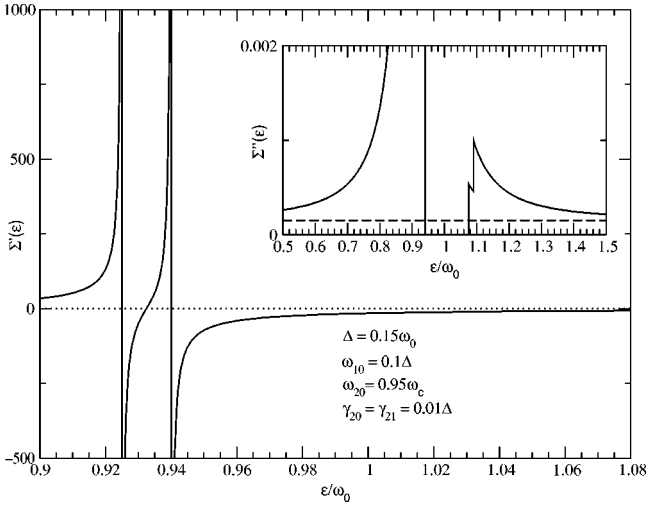

FIG. 6. The real part $\Sigma'(\epsilon)$ (solid curve) of the self-energy for a frequency dispersive medium as a function of the scaled frequency ϵ/ω_o. The quantities r, ω_{10}, ω_{20}, γ_{20}, and γ_{21} are the same as those in Fig. 3. The dotted line represents the real part of the free space self-energy, which is identically zero [see Eq. (26a)]. In the inset is shown a plot of the imaginary part $\Sigma''(\epsilon)$ (solid curve). The dashed line in the inset represents the imaginary part of the free space self-energy given by Eq. (26b). The scale used for plotting $\Sigma''(\epsilon)$ is much smaller than that used for plotting $\Sigma'(\epsilon)$.

$\Sigma'(\epsilon) = 0$. On the other hand, in the FDM case, $\Sigma'(\epsilon)$ increases from $-\infty$ to about $\Sigma'(\epsilon) = -20$ and is entirely negative in the frequency range G'.

In what follows we briefly discuss the discrete bound states and the continuous spectra of Secs. III D and III E in a frequency dispersive medium described by the dispersion relation (58). First we investigate the condition for the occurrence of a photon-atom bound state. As shown in Eq. (42), a discrete bound state is given by the eigenvalue ϵ satisfying $\Sigma'(\epsilon) = \omega_{20} - \epsilon$ provided that $\epsilon \in G' = (0.94,1.075)$. However, as shown in Fig. 6, in the frequency range G', $\Sigma'(\epsilon) < -20$. Thus to satisfy the equality $\Sigma'(\epsilon) = \omega_{20} - \epsilon$, we must have $\epsilon > \omega_{20} + 20$, which means that $\epsilon \notin G'$. In other words, Eq. (42) does not have a solution within the frequency range $G' = (0.94,1.075)$, where $\Sigma'' = 0$. In conclusion, for the choice of parameters in Sec. IV B used to support a photon-atom bound state in a PBG, a frequency dispersive medium does not support a photon-atom bound state.

Next we investigate equation (53) in the case of FDM. We choose the relevant parameters Δ, ω_{20}, γ_{20}, and γ_{21} just like in the PBG case (see Fig. 4). In Fig. 7 we plot the Rayleigh spectrum $\sigma_R(\omega)$ versus $\omega - \omega_{20}$ for various values of the Stokes transition frequency ω_{21} ($\omega_{21} = 1.15\omega_c$, $1.05\omega_c$, ω_c and ω_o). On the scale of the figure, all cases give the same spectral distribution which is ''half-Lorentzian'' cutoff at $\omega - \omega_{20} = 0.365$ (that is, at $\omega = 0.925 = \omega_v$). The peak value of this spectrum is less than that of free space (shown in the inset) by about three orders of magnitude.

Figure 7 is the FDM analog of Fig. 4. Comparing the two figures, we notice a number of differences. In the FDM case

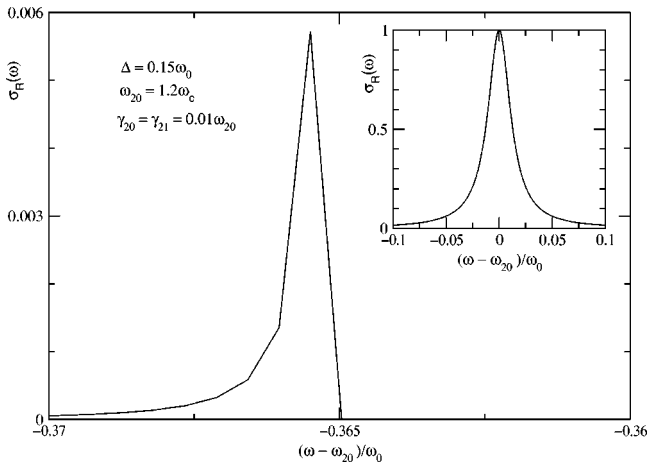

FIG. 7. The spectrum of spontaneous emission $\sigma_R(\omega)$ for the Rayleigh transition $|2\rangle \rightarrow |0\rangle$ in the case of FDM described by the isotropic dispersion relation (58). The parameters $r = 15\%$, ω_{20}, γ_{20}, and γ_{21} have the same values as in Fig. 4. We plot $\sigma_R(\omega)$ for different values of ω_{21} ($\omega_{21} = 1.15\omega_c$, $1.05\omega_c$, ω_c, and ω_o) of the Stokes frequency. On the scale of this figure, all cases give the same spectral distribution cutoff at $\omega = \omega_v$ and a peak value that is less than the free space case (shown in the inset) by about three orders of magnitude.

(unlike in the PBG case) there is no spectral splitting when ω_{21} lies close to the upper band edge ω_c. This can be explained by comparing the density-of-states near ω_c in the PBG and FDM cases, Figs. 2 and 5, respectively. In the PBG case the photon density-of-states near ω_c (on the upper side) is much greater than that of free space leading to strong atom-field interaction, resulting in level splitting. On the other hand, in the case of FDM the photon density-of-states in the neighborhood of ω_c is less than that of free space. In this case atom-field interaction in this frequency region is partially suppressed.

Another difference between Figs. 4 and 7 is that, in the PBG case the spectral distribution $\sigma_R(\omega)$ is very sensitive to small changes in ω_{21}, whereas in the FDM case all considered values of ω_{21} give essentially the same result. This can again be explained by referring to Figs. 2 and 5. As shown in Eq. (34), $\sigma_R(\omega)$ is proportional to $\rho(\omega)$ and therefore reflects the variation of the photon density-of-states with frequency. In the FDM case $\rho(\omega)$ varies little near ω_c whereas in the PBG case it is singular at ω_c. Finally, the peak of the spectral distribution is much larger in the PBG than in the FDM case. This can be explained by the fact that $\sigma_R(\omega) \propto \rho(\omega)$, as shown in Eq. (34).

The sensitivity of the Raman scattering cross section near the band edge of an isotropic dispersion relation is due to the rapid variation of the density-of-states near the band edge. A divergence in the density-of-states at both band edges of the isotropic PBG model, and at the lower band edge of the FDM model leads to large vacuum Rabi splitting [5]. This vacuum Rabi splitting is absent near the upper band edge of the FDM. Similarly, in a more realistic anisotropic PBG model, vacuum Rabi splitting is absent. However, both Rabi splitting and non-Markovian radiative dynamics reappear when an infinitesimal electromagnetic field is applied to the system. This may occur in the case of superradiance (collective light emission from a number of atoms) [8] or in the case of a very weak external field [12].

In conclusion, Raman scattering from a three-level atom in a PBG material sensitively depends on the positions of the Stokes transition frequency ω_{21} and the Rayleigh transition ω_{20} relative to the band-edge frequency ω_c. When both ω_{21} and ω_{20} are far above ω_c, the corresponding spectra are both Lorentzian as in free space. However, if either of the transition frequencies are close to ω_c, the spectra will be markedly different from the free space case. For example, if ω_{20} lies far above ω_c, while ω_{21} is near ω_c, the Rayleigh spectrum is split into triplets. The middle band that lies between $\omega_v + \omega_{10}$ and $\omega_c + \omega_{10}$ measures the fractionalized steady-state atomic population on the excited level $|2\rangle$. As $\omega_{21} \rightarrow \omega_c^+$, the dark lines shift upward in frequency and the width of the middle band increases. In this manner, resonance Raman scattering can be used as a direct experimental probe of the photon-atom bound state.

ACKNOWLEDGMENTS

This work was supported in part by the New Energy and Industrial Technology Development Organization (NEDO) of Japan, the Natural Sciences and Engineering Research Council of Canada, and Photonics Research Ontario.

APPENDIX: PHOTON DENSITY-OF-STATES IN PBG MATERIALS AND IN FREQUENCY DM

The photon density-of-states in a medium is defined by

$$\rho(\omega) = \frac{1}{L^d} \sum_{\mathbf{k}} \delta[\omega - \omega(\mathbf{k})], \tag{A1}$$

where L^d is the sample volume in d-dimensional space and $\omega(\mathbf{k})$ is the photon dispersion relation in the medium. In the limit of large L, we may replace the sum by the integral:

$$\rho(\omega) = \frac{1}{(2\pi)^d} \int d^d\mathbf{k}\, \delta[\omega - \omega(\mathbf{k})]. \tag{A2}$$

When the dispersion relation is isotropic [i.e., when $\omega(\mathbf{k})$ depends only on the magnitude k of $\mathbf{k}$] we can perform the angular integration in Eq. (A2) to obtain

$$\rho(\omega) = \frac{S_d}{(2\pi)^d} \int k^{d-1} dk\, \delta[\omega - \omega(k)], \tag{A3}$$

where S_d is the surface area of a unit sphere in d dimensions ($S_d = 2, 2\pi$ or 4π for $d = 1, 2$ or 3, respectively). Using Eq. (8) in Eq. (A3) we obtain

$$\delta[\omega - \omega(k)] = z(\omega)\, \delta[k - k(\omega)], \tag{A4}$$

and inserting this in Eq. (A3) we finally obtain

$$\rho(\omega) = \frac{S_d}{(2\pi)^d} k^{d-1}(\omega) z(\omega) \tag{A5}$$

for the density-of-states in d dimensions. In free space $k(\omega)=\omega$ so that $z(\omega)=1$. In $d=3$ this yields $\rho(\omega)=\omega^2/2\pi^2$ for the free space photon density-of-states.

For a PBG, we use the dispersion relation (54) to obtain

$$z(\omega)=\frac{|\omega-\omega_o|}{\sqrt{(\omega-\omega_v)(\omega-\omega_c)}}. \tag{A6}$$

Clearly, $z(\omega)$ exhibits square-root singularities at the band-edge frequencies ω_v and ω_c. From Eqs. (54) we obtain

$$k(\omega)=\sqrt{\omega_v\omega_d}\pm\sqrt{(\omega-\omega_c)(\omega-\omega_v)}, \tag{A7}$$

where the $+(-)$ sign applies for $\omega>\omega_c$ $(\omega<\omega_v)$. Equation (A7) shows that, for the frequency range $G\equiv(\omega_v,\omega_c)$ spanning the gap, the wave vector $k(\omega)$ is complex, indicating that the wave is nonpropagating. Outside the PBG (that is, for $\omega\notin G$) Eqs. (A7), (A6), and (9) give

$$\rho(\omega\notin G)=\frac{|\omega-\omega_o|}{2\pi^2}\left[\frac{\omega^2-2\omega_o\omega+2\omega_v\omega_c}{\sqrt{(\omega-\omega_v)(\omega-\omega_c)}}\pm 2\sqrt{\omega_v\omega_c}\right], \tag{A8}$$

where the $+(-)$ sign applies for $\omega>\omega_c$ $(\omega<\omega_v)$.

For a dispersive medium, described by the dispersion relation (58) we obtain

$$k(\omega)=\omega\left(\frac{\omega-\omega_c}{\omega-\omega_v}\right), \tag{A9}$$

where $\omega_v=\Omega-\Delta$ and $\omega_c=\Omega$ are the band-edge frequencies. The form factor $z(\omega)$ of the medium is then given by

$$z(\omega)=\frac{\omega^2-2\omega_v\omega+\omega_v\omega_c}{(\omega-\omega_v)^2}. \tag{A10}$$

Unlike in the PBG case, where $z(\omega)$ is singular at both band-edge frequencies, in the FDM case $z(\omega)$ is singular only at the lower band-edge frequency ω_v. Moreover, the singularity at ω_v is much stronger $z(\omega)\sim(\omega-\omega_v)^{-2}$ than that in the PBG case.

The wave number k, being the magnitude of a vector $(\mathbf{k})$, is positive definite. However, Eq. (A9) shows that, for frequencies $\omega\in G$, $k(\omega)$ is negative, indicating that this range corresponds to the PBG region. Outside the photonic band gap, Eqs. (A9), (A10), and (9) give

$$\rho(\omega\notin G)=\frac{\omega^2(\omega-\omega_c)^2}{2\pi^2}\left[\frac{\omega^2-2\omega_v\omega+\omega_v\omega_c}{(\omega-\omega_v)^4}\right], \tag{A11}$$

for the density-of-states in a frequency dispersive medium.

[1] E. Yablonovitch, Phys. Rev. Lett. **58**, 2059 (1987).
[2] S. John, Phys. Rev. Lett. **58**, 2486 (1987).
[3] E. Yablonovitch, T.J. Gimitter, and K.M. Leung, Phys. Rev. Lett. **67**, 2295 (1991).
[4] S. John, Phys. Rev. Lett. **53**, 2169 (1984).
[5] S. John and J. Wang, Phys. Rev. Lett. **64**, 2418 (1990); Phys. Rev. B **43**, 12 772 (1991); S. John, in *Confined Electrons and Photons*, edited by by E. Burstein and C. Weisbuch (Plenum, New York, 1995).
[6] S. John and T. Quang, Phys. Rev. A **50**, 1764 (1994).
[7] R.F. Nabiev, P. Yeh, and J.J. Sanchez-Mondragon, Phys. Rev. A **47**, 3380 (1993).
[8] S. John and T. Quang, Phys. Rev. Lett. **74**, 3419 (1995).
[9] S. John and T. Quang, Phys. Rev. A **52**, 4083 (1995).
[10] N. Vats and S. John, Phys. Rev. A **58**, 4168 (1998).
[11] S. John and T. Quang, Phys. Rev. Lett. **78**, 1888 (1997).
[12] M. Florescu and S. John (unpublished).
[13] S. John and V. I. Rupasov, Phys. Rev. Lett. **79**, 821 (1997); Europhys. Lett. **46**, 326 (1999).
[14] V.I. Rupasov and M. Singh, Phys. Lett. A **222**, 258 (1996); J. Phys. A **29**, L205 (1996).
[15] V.I. Rupasov and M. Singh, Phys. Rev. A **56**, 898 (1997).
[16] L.D. Landau and E.M. Lifshitz, *Electrodynamics of Continuous Media* (Pergamon, Oxford, 1984).
[17] V.M. Agranovich and V.L. Ginzburg, *Crystal Optics with Spatial Dispersion and Excitons* (Springer-Verlag, Berlin, 1984).
[18] L. Allen and J.H. Eberly, *Optical Resonance and Two-Level Atoms* (Wiley, New York, 1975).
[19] M. Woldeyohannes, S. John, and V. I. Rupasov (unpublished).
[20] J.J. Sakurai, *Modern Quantum Mechanics* (Addison-Wesley, New York, 1994).
[21] G.B. Arfken and H.J. Weber, *Mathematical Methods for Physicists* (Academic, New York, 1995).
[22] W.H. Louisell, *Quantum Statistical Properties of Radiation* (Wiley, New York, 1973).
[23] H.A. Bethe, Phys. Rev. **72**, 339 (1947).
[24] M. Woldeyohannes and S. John, Phys. Rev. A (to be published).
[25] K. Busch and S. John, Phys. Rev. E **58**, 3896 (1998), and references therein.
[26] Shi-Yao Zhu, Ricky C.F. Chan, and Chin Pang Lee, Phys. Rev. A **52**, 710 (1995).
[27] S. H. Autler and C. H. Townes, Phys. Rev. **100**, 703 (1955).
[28] E. Paspalakis, D.G. Angelakis, and P.L. Knight, Opt. Commun. **172**, 229 (1999).